ACS APPLIED MATERIALS & INTERFACES

Research Article

www.acsami.org

In Situ Transmission Electron Microscopy Observation of Electrochemical Behavior of CoS_2 in Lithium-Ion Battery

Qingmei Su,[†,‡] Jian Xie,[§] Jun Zhang,[†] Yijun Zhong,[†] Gaohui Du,*[,†] and Bingshe Xu[‡]

[†]Institute of Physical Chemistry, Zhejiang Normal University, Jinhua 321004, China

[‡]College of Materials Science and Engineering, Taiyuan University of Technology, Taiyuan 030024, Shanxi, China

[§]State Key Laboratory of Silicon Materials and Department of Materials Science and Engineering, Zhejiang University, Hangzhou 310027, China

Supporting Information

ABSTRACT: Metal sulfides are a type of potential anode materials for lithium-ion batteries (LIBs). However, their electrochemical behaviors and mechanism during the charge and discharge process remain unclear. In the present paper, we use CoS_2 as a model material to investigate their electrochemical process using in situ transmission electron microscopy (TEM). Two kinds of reaction behaviors are revealed. The pure CoS_2 particles show a side-to-side conversion process, in which large and anisotropic size expansion (47.1%) occurs that results in the formation of cracks and fractures in CoS_2 particles. In contrast, the CoS_2 particles anchored on reduced graphene oxide (rGO) sheets exhibit a core−shell conversion process involving small and homogeneous size expansion (28.6%) and few fractures, which attributes to the excellent Li^+ conductivity of rGO sheets and accounts for the improved cyclability. Single-crystalline CoS_2 particle converts to Co nanocrystals of 1−2 nm embedded within Li_2S matrix after the first lithiation. The subsequent electrochemical reaction is a reversible phase conversion between Co/Li_2S and CoS_2 nanocrystals. Our direct observations provide important mechanistic insight for developing high-performance conversion electrodes for LIBs.

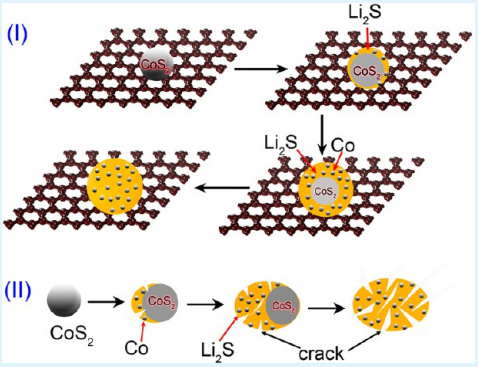

KEYWORDS: *lithium-ion battery, cobalt sulfide, reduced graphene oxide, in situ TEM, anode*

1. INTRODUCTION

Lithium-ion batteries (LIBs) are widely used as power devices for portable electronics, electric vehicles, and the storage of renewable energy.[1,2] Because of the rapid development of such applications, LIBs with superior energy density, power density, and good cyclability are required.[3,4] After the report by Whittingham in 1976 of reversible Li insertion into TiS_2 for the cathode reaction of LIBs,[5] many other transition metal dichalcogenides (or nitrides, phosphides, and fluorides) have been extensively investigated for LIBs.[6−8] Cobalt sulfide represents one of the most promising anode materials for the next-generation LIBs, as it has a high theoretical lithium storage capacity (870 mAh/g for CoS_2),[9] which is larger than that of the carbonaceous anodes (372 mAh/g) currently used in commercial LIBs. However, large volume expansion of electrode materials during the discharge/charge process in the first cycle remains a serious issue leading to cracking, fracture, and electrical disconnection from current collectors, which have been recognized as one of the major causes for rapid capacity fading in LIBs.[10−14]

A few methods have been developed to mitigate these negative effects for better capacity retention, for instance, by constructing nanoscale materials,[15] coating the high-capacity material by carbon,[16] or adding an elastomeric binder as a buffer to adapt the volume expansion.[17] Graphene or reduced graphene oxide (rGO) sheets are considered as an effective buffering matrix to disperse nanoparticles, and the obtained composites are very promising for using as anode materials in LIBs. For example, it was reported that metal oxide (or sulfide)/rGO composites show increased capacitance and improved cyclability as compared to the pure metal oxide (or sulfide) electrode.[18−21] The improvement of electrochemical performances has been mainly attributed to the excellent mechanical and electronic properties of rGO nanosheets. It is still not fully understood whether and how rGO sheets influence the electrochemical behavior of the loaded nanostructures. The intrinsic relationship between the structure and the electrochemical performance remains unclear so far because of the lack of effective characterization technique. Recently, a few in situ techniques[22,23] have been developed to monitor the electrochemical process in LIBs. Among these methods, in situ TEM is much more powerful to real time reveal the electrochemical process of the electrode materials during cycling, and provide detailed information on morphology and

Received: December 6, 2013
Accepted: January 16, 2014
Published: January 16, 2014

   dx.doi.org/10.1021/am4056084 | ACS Appl. Mater. Interfaces 2014, 6, 3016−3022

phase evolution during electrochemical reaction with high spatial resolution. Recently, some successes have been achieved on understanding the electrochemical processes of SnO_2,[24] Si,[25] ZnO,[26] CeO_2,[27] Fe_2O_3,[28] carbon nanotube (CNT),[29] graphene,[30] and Co_9S_8/CNT[31] through the in situ TEM technique.

Graphene-based composites are a kind of important electrode materials in LIBs. However, the electrochemical process of the kind of materials is not well understood; in particular, the interaction between the graphene-based substrate and the loaded nanostructures remain unclear. To solve this issue, we constructed an all-solid nano-LIB in the present study using CoS_2/rGO as working electrode inside a high-resolution TEM to enable the in situ observation of the dynamic charge−discharge processes. We performed a comparative study of the electrochemical behaviors of pure CoS_2 particle and CoS_2/rGO using in situ TEM, and the role of rGO sheets in enhancing the electrochemical performance of electrode materials is revealed.

2. EXPERIMENTAL SECTION

2.1. Preparation of CoS_2/rGO and CoS_2. The CoS_2/rGO composites were synthesized by a facile one-step hydrothermal route using graphite oxide, thioacetamide, and $CoCl_2 \cdot 6H_2O$ as raw materials.[32] Pure CoS_2 powders were also prepared by this method without the addition of graphite oxide.

2.2. In Situ Electrochemical Experiments. The in situ nanoscale electrochemical experiments were performed in a TEM (JEOL JEM-2100F) with a Nanofactory TEM-STM holder. The CoS_2/rGO powders were attached to a gold wire with a clean and fresh cross section, which was used as the working electrode. A tungsten wire cut by a scissor was used to scratch Li metal surface to fetch some fresh Li inside a glovebox filled with argon, and the Li metal attached to the tungsten wire was served as the counter electrode. During the TEM-STM holder loading process, the Li metal was exposed to air for a short time, which led to the natural formation of Li_2O. The resultant Li_2O layer was used as a solid electrolyte allowing Li^+ transport. The Li_2O/Li electrode was mounted on the mobile STM probe, which was driven to contact the working electrode by a piezo-positioner inside the TEM. The electrochemical reaction took place after a bias was applied on the working electrode with respect to the lithium metal to drive Li^+ ions transport through the solid-state Li_2O layer. During the experiments, the electron beam was blanked except for short time beam exposure for imaging to minimize the electron beam irradiation effect during the reaction.

2.3. Half Cell Measurement. The electrochemical cycling experiments were performed at a CT2001A Land battery tester at room temperature. To prepare the LIB anode, the electrode slurry was made by mixing the active material, acetylene black, and polyvinylidene fluoride (PVDF) in a weight ratio of 75:15:10 in N-methyl pyrrolidone with stirring for 2 h, then the slurry was spread onto a Ni foam current collector and dried at 120 °C under vacuum overnight. The electrolyte solution was 1 M $LiPF_6$ dissolved in ethylene carbonate/dimethyl carbonate (1:1, v/v). The CR2025-type coin cells were assembled in an argon-filled glovebox using pure Li foil (Aldrich) as the counter electrode. The cells were charged and discharged between 0.01 and 3 V (vs Li/Li^+) at a current density of 50 mA g^{-1}.

3. RESULTS AND DISCUSSION

Figure 1a displays the experiment setup of the nanoscale electrochemical device constructed inside the TEM. Briefly, the electrochemical nano-LIB device consists of an individual CoS_2/rGO electrode, a layer of Li_2O solid electrolyte, and a bulk Li counter electrode. The TEM image of the nano-LIB inside the TEM is shown in Figure 1b. The Li_2O/Li electrode mounted on the mobile STM probe was driven to contact the

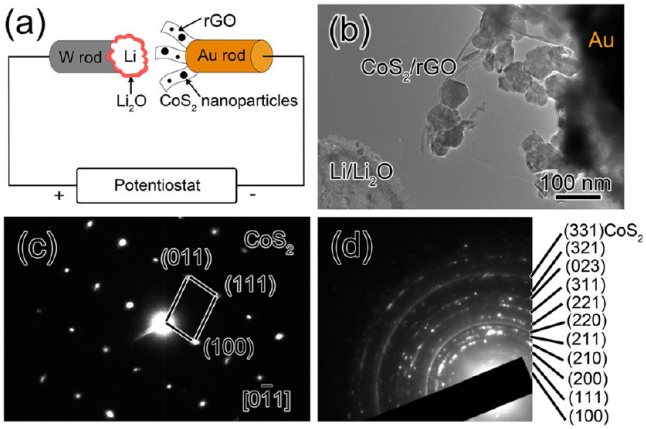

Figure 1. (a) Schematic illustration of the in situ experimental setup inside a TEM. (b) The corresponding TEM image of the nano-LIB constructed inside the TEM. (c) EDP pattern of a single Co_2S nanoparticle anchored on the rGO sheet. (d) EDP of a region containing many Co_2S nanoparticles on the rGO sheet.

CoS_2/rGO electrode. To initiate the lithiation process, a potential of −1 V was applied on the CoS_2/rGO with respect to the lithium metal to drive Li^+ transport through the solid-state Li_2O layer; the bias was reversed to positive (+3 V) to facilitate the delithiation reaction. The electron diffraction pattern (EDP) recorded from a single particle anchored on the rGO sheet displays regular diffraction spots (Figure 1c), and it can be indexed as cubic CoS_2 along the [0$\bar{1}$1] zone axis. The EDP analyses indicate the single crystalline nature of CoS_2 nanoparticles. The EDP recorded from a region containing many particles is shown in Figure 1d. The dominant diffraction rings can be indexed as the pure cubic CoS_2 in agreement with the JCPDS No. 89−3056.

The morphological evolution and phase transformation of CoS_2 particles on rGO sheets during the first lithiation are show in Figure 2 and Movie S1 in the Supporting Information. A pristine CoS_2 nanoparticle was 152 nm as shown in Figure 2a. After the lithiation was initiated for 28 s (Figure 2b), the CoS_2 nanoparticle began to react with Li^+ ions. Gray-contrasted shells were forming on the CoS_2 particles, indicating a fast lithiation occurred on the particle surface. The Li^+ ions appeared to move quickly on the surface of rGO sheet and then reacted with the CoS_2 nanoparticles (Figure 2c). Lithiation resulted in a sequential morphology evolution of CoS_2 from the surface inward to the core quickly as the lithiation continued. Figure 2c−f displays the continuous electrochemical behavior of CoS_2 particles in the lithiation process. Figure 2g is a TEM image of the electrode recorded after the lithiation reaction was complete, in which the marked CoS_2 nanoparticle expanded from 152 to 192 nm in size, corresponding to ∼26.3% size expansion. Figure 2h shows a HRTEM image of a fully lithiated CoS_2 particle, which consists of many nanograins around 2 nm. A few nanograins with the fringe spacing of 0.20 nm are agreed with the crystalline Co. The fringe spacing of 0.33 nm can be indexed as the (111) planes of Li_2S. The EDP of the lithiated CoS_2/rGO electrode is shown in Figure 2i; the diffraction rings can be perfectly indexed as a mixture of face-centered cubic (fcc) Co (JCPDS no. 89−4307) and fcc Li_2S (JCPDS no. 77−2145). It reveals the lithiation reaction of CoS_2 particles involves the conversion from CoS_2 phase to Co and Li_2S. These direct experimental observations reveal that the lithiation initiates at the surface and then propagates into the core with

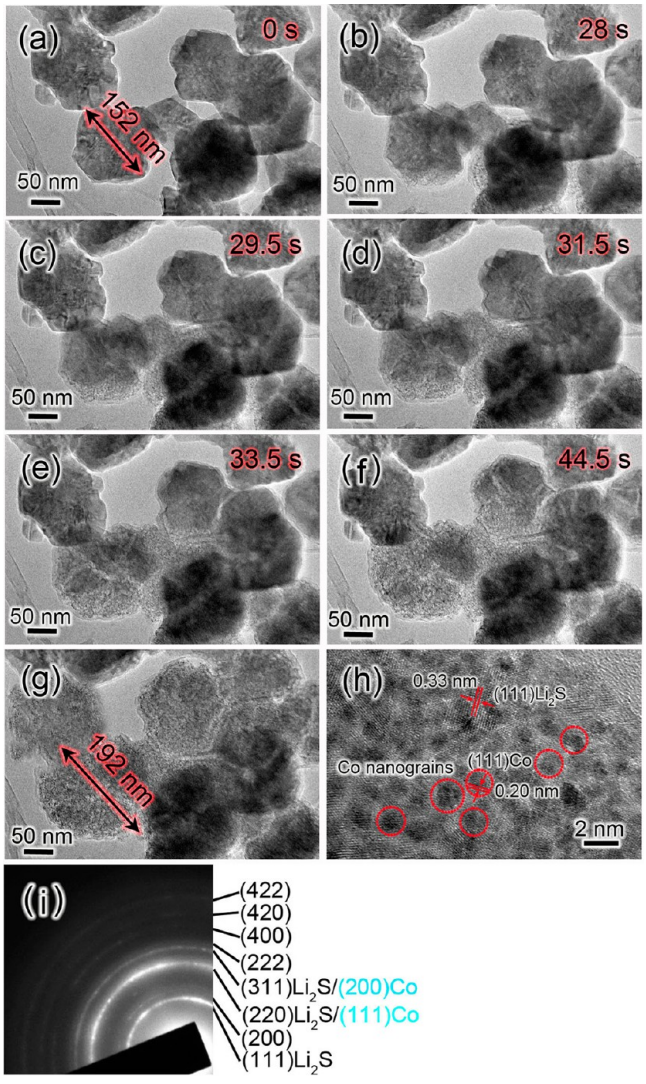

Figure 2. Time-resolved TEM images from video frames show the electrochemical lithiation of CoS_2 nanoparticles anchored on rGO sheets. (a) Pristine CoS_2 particles. (b–f) Time sequence of the electrochemical lithiation of CoS_2 nanoparticles. (g) TEM image of the fully lithiated CoS_2 particles. (h) HRTEM image of a lithiated CoS_2 nanoparticle. (i) EDP of the lithiated CoS_2/rGO electrode showing the phase conversion.

obvious volume expansion. TEM analysis suggests the formation of Co metal nanograins of 1–2 nm embedded in the Li_2S matrix after the first lithiation. Therefore, the first lithiation of CoS_2 nanoparticles as anode can be expressed as the electrochemical reaction: $CoS_2 + 4Li^+ + 4e^- \rightarrow Co + 2Li_2S$. The CoS_2 particles anchored on rGO sheets show no notable cracks and fractures and display stable behavior during the electrochemical lithiation process despite the volume expansion of ~101.5% was observed by the in situ TEM study.

To investigate the effect of rGO sheets on the lithiation reaction of loaded nanostructures, we used an individual CoS_2 particle without rGO sheets as the working electrode inside TEM, and its morphological evolution during lithiation is shown in Figure 3 and Movie S2 in the Supporting Information. This CoS_2 particle was about 226 nm in size (Figure 3a). After lithiation for 14 s (Figure 3b), a thin gray-contrasted layer formed on the CoS_2 surface, indicating the start of lithiation on the CoS_2 nanoparticle. The lithiation of pure CoS_2 nanoparticle was found to be notably anisotropic, showing the gradual structural change along the Li^+ diffusion direction from the Li_2O/Li electrode toward the Au electrode (as shown in Figure 3c–i). In particular, some cracks nucleated and grew on the surface of CoS_2 nanoparticle (indicated by red arrows) and propagated toward the Au electrode quickly as the lithiation continued. The growth of multiple cracks at different locations led to the fracture of the CoS_2 particle eventually (Figure 3l). This is similar with the previously reported morphological evolution of Si particles with the diameter above the critical size of 150 nm during electrochemical lithiation.[33] During the lithiation process, the reaction front propagated from the left to the right of the particle, leading to a lateral expansion from 226 to 326 nm (Figure 3l), corresponding to ~53.1% size expansion; meanwhile, the size of the particle increased to 214 nm from 196 nm in the longitudinal direction, corresponding to a size expansion of ~9.2%. So the pure CoS_2 particle exhibited large and anisotropic expansion. The lithiation processes of about fifteen CoS_2 particles were examined, and we found the anisotropic expansion was not relevant with the crystal orientation of each particle but determined by the uneven lithiation reaction. The severe cracking and fracturing observed during the lithiation can unavoidably result in a loss of electric connectivity and even the exfoliation of the active materials from current collectors, causing a rapid capacity fading in real battery. In contrast to the lithiation process of CoS_2 anchored on rGO sheets, it suggested that the use of flexible rGO sheets can effectively alleviate the cracking of CoS_2 in the first electrochemical lithiation by achieving a homogeneous reaction, which is beneficial for the electrochemical cycling and the capacity retention.

The behavior of CoS_2/rGO anode during the electrochemical lithiation-delithiation cycling was further investigated using in situ TEM. Detailed structure and phase evolutions during the first two lithiation-delithiation cycles are shown in the TEM images (Figure 4a–e) and EDPs (Figure $4a_1$–e_1). A typical CoS_2 nanoparticle anchored on rGO sheets with a size of ~124.2 nm is shown in Figure 4a. The corresponding EDP of the pristine CoS_2/rGO electrode is displayed in Figure $4a_1$, which is well in agreement with the fcc CoS_2 (JCPDS no. 89–3056). After the first lithiation process (Figure 4b), the lithiated nanoparticle expanded to 154.6 nm, corresponding to a size expansion of ~24.5%. The corresponding EDP of the lithiated electrode is shown in Figure $4b_1$; the diffraction rings can be well indexed to fcc Co and fcc Li_2S, suggesting the conversion of CoS_2 to Co in the first lithiation process. Then the delithiation process was initiated by reversing the potential from −1 V to +3 V. The lithiated nanoparticle shrunk gradually and reduced to ~130.2 nm after delithiation (Figure 4c). We found ~4.83% of the size expansion is irreversible due to microstructural change compared with the pristine single-crystalline CoS_2 particle. The fully delithiated phase was identified to be CoS_2 by EDP analysis of the delithiated electrode as shown in Figure $4c_1$. Although the delithiated particle is still CoS_2, it consists of numerous CoS_2 nanograins of ~5 nm. After the first cycle, the second lithiation process proceeded with the −1 V potential, and the similar volume expansion was observed again (Figure 4d); the marked particle expanded to about 152.2 nm. The EDP of the second lithiated particle was shown in Figure $4d_1$, which revealed that Co and Li_2S were also the lithiated product. The volume shrank was further observed in the second delithiation process with the potential of +3 V (Figure 4e), and the EDP shown in Figure $4e_1$

dx.doi.org/10.1021/am4056084 | ACS Appl. Mater. Interfaces 2014, 6, 3016–3022

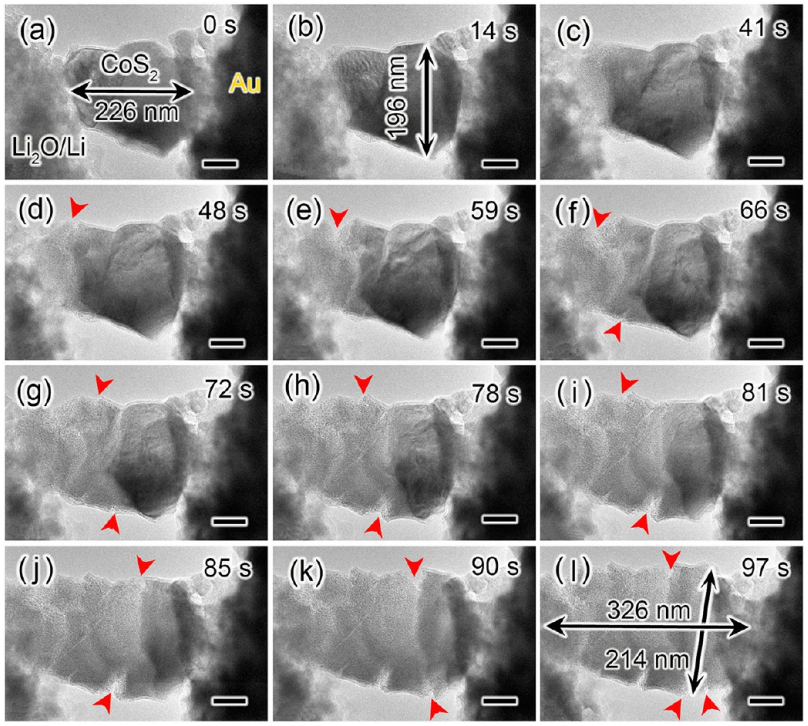

Figure 3. Time-resolved TEM images from video frames show the electrochemical lithiation of a single CoS_2 particle without rGO sheets under a potential of −1 V. (a) Pristine CoS_2 particle with a size of about 226 nm. (b–l) Time sequence of the lithiation process showing the crack initiation and growth in the lithiated particle. Scale bars are 50 nm.

suggested the conversion from Co/Li_2S to CoS_2 again in the delithiation process. It is worth mentioning that the CoS_2 particle remains intact during the lithiation/delithiation cycling without obvious cracks and fractures, which is beneficial for the electrical contact. The in situ TEM results displayed that the nature of CoS_2 in LIBs is a reversible conversion between CoS_2 and Co/Li_2S. The electrochemical reaction of CoS_2 in LIBs can be expressed as $CoS_2 + 4Li^+ + 4e^- \leftrightarrow Co + 2Li_2S$. The lithiation reaction pertains to the conversion mechanism as reported for metal oxides and fluoride.[34,35]

The previous study showed that the fracture of Si nanoparticles is size-dependent; namely, the surface cracks nucleated and propagated in Si nanoparticles above a threshold size of ∼150 nm in diameter upon the first lithiation.[33] To investigate whether there is a correlation between the fracture and the particle size for CoS_2, we compared the lithiation of 15 pure CoS_2 particles and 15 CoS_2 particles anchored on rGO sheets. The statistic results are shown in Figure 5. The size expansion of CoS_2 nanoparticles anchored on rGO sheets ranges from 20 to 35% with a mean value of 28.6%. Contrarily, the size expansion (along the Li^+ diffusion direction) of pure CoS_2 particles range from 41 to 55% with a mean value of 47.1%, which is much larger than that of CoS_2 nanoparticles on rGO sheets. The larger expansion in pure CoS_2 particles is attributed to the anisotropic expansion and the formation of obvious fractures in the particles as observed by TEM. We found that the crack and fracture of CoS_2 nanoparticles was independent of their particle size but they can be alleviated by the rGO substrate. A strong size dependence of fracture was discovered in the lithiation of Si particles.[33] The surface cracking in large particle can be attributed to the buildup of large tensile hoop stress in the surface layer induced by the "push-out" effect due to the volume expansion of materials at the interior. The small-sized nanoparticles never fracture because the stored strain energy from electrochemical reactions is insufficient to drive crack propagation. As for the CoS_2 particles, they abide by a conversion mechanism as anode in LIBs, which is different with the alloying mechanism of Si. The volume expansion of CoS_2 after lithiation is around 100%, which is much smaller than that of Si (∼300%). Therefore, the resulted tensile hoop stress in the surface layer of the lithiated CoS_2 would be much smaller than that in the lithiated Si particle under the same condition, which can account for the different electrochemical behavior of CoS_2 as compared to Si particles.

According to the in situ TEM study by constructing a nano-LIB device inside TEM, the electrochemical lithiation process of CoS_2 should proceed as illustrated in Figure 6. As for the CoS_2 nanoparticles anchored on rGO sheets during the first lithiation process (Figure 6a), Li^+ ions can diffuse quickly on rGO sheet,[30] which ensures a comparatively uniform lithiation in CoS_2 particles. The Co/Li_2S shells are initially formed on CoS_2 particles during lithiation, and then penetrate inward to the core gradually, suggesting a core–shell conversion model. In the homogeneous lithiation process, the CoS_2 nanoparticles show no severe cracks and fractures because the reaction fronts (two phase boundary) shrink and the resultant strain and stress reduce gradually as the lithiation proceeds. In other words, the good Li^+ conductivity of rGO sheets make the lithiation of CoS_2 particles homogeneously, which benefits for the relief of strain and stress. In a real battery, the stacking of rGO sheets can generate a porous network in electrode, providing excellent electron-conducting and ion-transporting pathways. The porous structures can further buffer the volume expansion of the loaded materials and avoid large stress, which is crucial for improving the reversible capacity. As for pure CoS_2 particles, the lithiation takes place and propagates from one side to another side of the particles as the reaction continues, revealing

dx.doi.org/10.1021/am4056084 | ACS Appl. Mater. Interfaces 2014, 6, 3016–3022

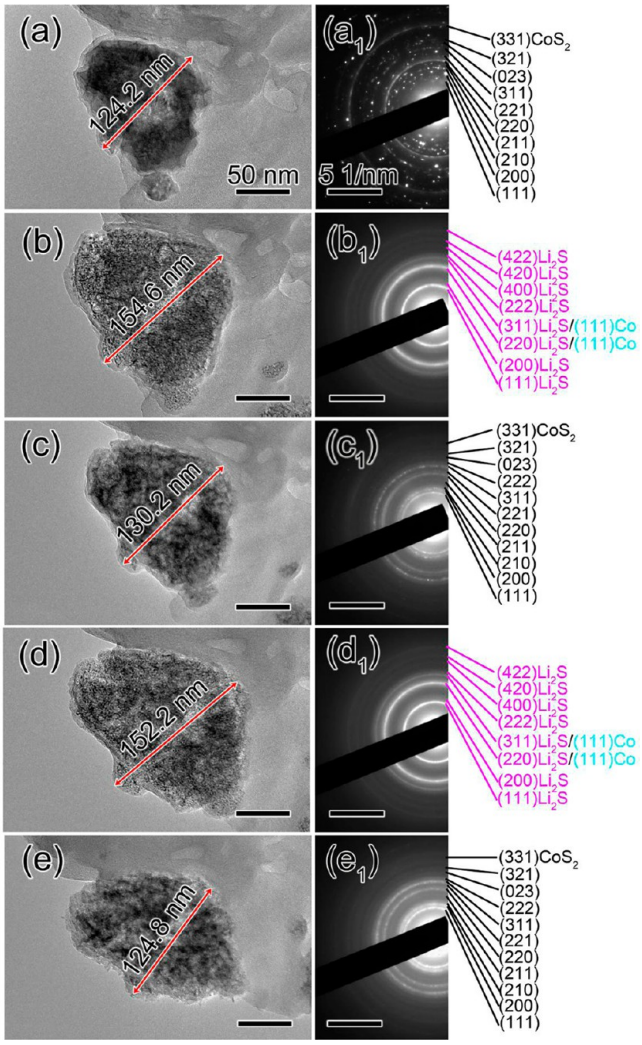

Figure 4. Microstructure evolution of CoS_2/rGO in the lithiation and delithiation processes during the first two cycles. (a) Typical pristine CoS_2 particle anchored on rGO sheets with a size of 124.2 nm. (b) First lithiated and (c) delithiated CoS_2. (d) Second lithiated and (e) delithiated CoS_2. (a_1–e_1) EDPs of the electrode in (a–e) revealing the reversible transformation between CoS_2 and Co/Li_2S.

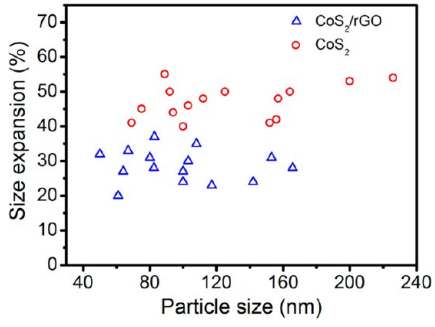

Figure 5. Statistics showing the relationship between the expansion and the particle size.

a side-to-side conversion process as illustrated in Figure 6b. In this conversion mode, the reaction fronts during the lithiation are large for the most time except for the beginning and ending stages. Some cracks grow and nucleate near the reaction fronts, where there is huge stress owing to the volume expansion. As the lithiation continues, the growth of multiple cracks at

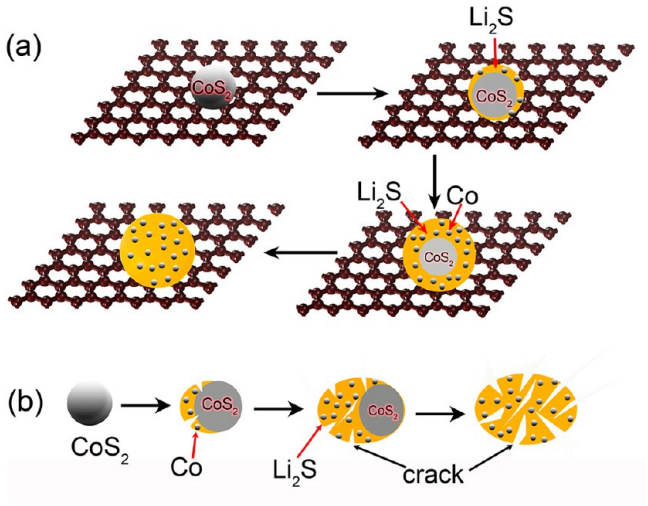

Figure 6. Schematic drawing showing the electrochemical lithiation process. (a) CoS_2 particles anchored on rGO sheets show a core–shell conversion process; (b) pure CoS_2 particles show a side-to-side conversion process.

different locations lead to the fracture of the particles, which can result in the poor electric contact of particles and thus cause capacity fading of the electrode material in LIBs. Although this reaction mode is revealed by in situ TEM observation of individual particles, it can be applied in the situation in real battery, in which pure metal oxide or sulfide particles are easily aggregated so lithiation is not proceeding homogeneously. In particular, large stress occurs among the particles during lithiation because of volume expansion, which aggravates the cracking and pulverization of the electrode.

The cycling performances of CoS_2 and CoS_2/rGO as anode were examined in coin-type half cell configuration at a current density of 50 mA g^{-1} to correlate the macroscopic electrochemical properties with the microcosmic TEM results. As shown in Figure 7, the pure CoS_2 electrode delivers a discharge

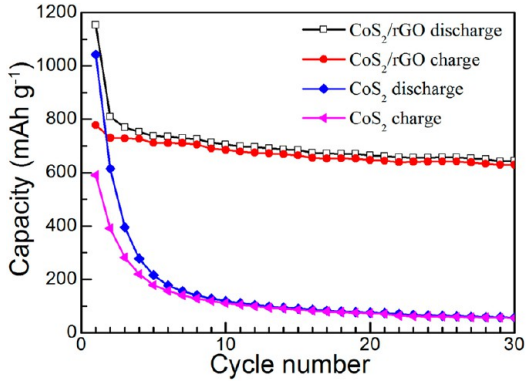

Figure 7. Cycling performance of the CoS_2/rGO and pure CoS_2 electrodes at a current density of 50 mA g^{-1} in LIBs.

and charge capacity of 1042 and 590 mAh g^{-1}, respectively, with a Coulombic efficiency of 56.6%. Its reversible capacity decreases rapidly in the first 10 cycles and stabilizes at 57 mAh g^{-1} after 30 cycles. In contrast, the CoS_2/rGO electrode exhibits high reversible capacity and excellent cycling stability. The CoS_2/rGO delivers an initial discharge capacity of 1154 mAh g^{-1} and a charge capacity of 778 mAh g^{-1} in the first cycle with a Coulombic efficiency of 67.4%. The reversible capacity

dx.doi.org/10.1021/am4056084 | ACS Appl. Mater. Interfaces 2014, 6, 3016–3022

of CoS_2/rGO exhibits gentle decrease since the second cycle and retains 644 mAh g^{-1} after the 30th cycle, which is almost eleven times higher than that of pure CoS_2 electrode. The initial capacity fading of CoS_2 electrode is 452 mAh g^{-1} in the first cycle, which is obviously larger than that of the CoS_2/rGO electrode (~376 mAh g^{-1}) because of a huge crack and pulverization as we observed by in situ TEM. The pure CoS_2 delivers only 6.6% of its theoretical capacity (870 mAh g^{-1}) in the 30th cycle, indicating about 93.4% of CoS_2 does not participate in the electrochemical reaction any more because of the electrode pulverization.

4. CONCLUSIONS

In summary, the electrochemical lithiation and delithiation behaviors of individual CoS_2 was studied by constructing a nano-LIB inside a TEM. The direct observation confirmed that the electrochemical process of CoS_2 in LIBs involves a reversible phase conversion between CoS_2 and Co/Li_2S. The formation of Co nanograins of 1−2 nm within the Li_2S matrix is observed during the lithiation process. By comparing the lithiation of CoS_2/rGO with pure CoS_2, we found that the CoS_2 particles on rGO sheets demonstrate a core−shell conversion process with small and homogeneous expansion while pure CoS_2 particles shows a side-to-side conversion, in which the CoS_2 particles have large and anisotropic expansion with the formation of obvious cracks and fractures. The results suggest that rGO sheets can cause a homogeneous lithiation of the loaded nanoparticles by transporting Li^+ quickly, which is beneficial for the capacity retention of electrode materials in LIBs. The half cell measurements reveal that the reversible capacity of CoS_2/rGO is almost eleven times higher than that of pure CoS_2 electrode after 30 cycles, confirming the important role of rGO sheets in enhancing the electrochemical performance by preventing the loaded nanostructures from fracturing. Two kinds of conversion modes are revealed for CoS_2 electrode by the in situ TEM observation, which could be applied to other metal oxide/sulfide electrodes. These findings provide direct experimental evidence for the understanding and design of high-performance electrode materials.

■ ASSOCIATED CONTENT

Supporting Information

Two movies show the lithiation process of individual CoS_2 nanoparticles anchored on rGO sheets and a pure CoS_2 particle. This material is available free of charge via the Internet at http://pubs.acs.org.

■ AUTHOR INFORMATION

Corresponding Author

*E-mail: gaohuidu@zjnu.edu.cn.

Notes

The authors declare no competing financial interest.

■ ACKNOWLEDGMENTS

This work was supported by the Program for New Century Excellent Talents in University of Ministry of Education of China (NCET-11-1081) and the National Science Foundation of China (1203168).

■ REFERENCES

(1) Armand, M.; Tarascon, J. M. *Nature* **2008**, *451*, 652.
(2) Wang, B.; Chen, J. S.; Wu, H. B.; Wang, Z.; Lou, X. W. *J. Am. Chem. Soc.* **2011**, *133*, 17146−17148.
(3) Tarascon, J. M.; Armand, M. *Nature* **2001**, *414*, 359−367.
(4) Service, R. F. *Science* **2011**, *332*, 1494−1496.
(5) Whittingham, M. S. *Science* **1976**, *192*, 1126−1127.
(6) Zhang, D.; Mai, Y. J.; Xiang, J. Y.; Xia, X. H.; Qiao, Y. Q.; Tu, J. P. *J. Power Sources* **2012**, *217*, 229−235.
(7) Ni, S. B.; Yang, X. L.; Li, T. *J. Mater. Chem.* **2012**, *22*, 2395−2397.
(8) Lu, Y.; Tu, J. P.; Xiong, Q. Q.; Xiang, J. Y.; Mai, Y. J.; Zhang, J.; Qiao, Y. Q.; Wang, X. L.; Gu, C. D.; Mao, S. X. *Adv. Funct. Mater.* **2012**, *22*, 3927−3935.
(9) Wang, Y. M.; Wu, J. J.; Tang, Y. F.; Lü, X. J.; Yang, C. Y.; Qin, M. S.; Huang, F. Q.; Li, X.; Zhang, X. *ACS Appl. Mater. Interfaces* **2012**, *4*, 4246−4250.
(10) Zhao, K. J.; Pharr, M.; Wan, Q.; Wang, W. L.; Kaxiras, E.; Vlassak, J. J.; Suo, Z. G. *J. Electrochem. Soc.* **2012**, *159*, A238−A243.
(11) Huang, J. Y.; Zhong, L.; Wang, C. M.; Sullivan, J. P.; Xu, W.; Zhang, L. Q.; Mao, S. X.; Hudak, N. S.; Liu, X. H.; Subramanian, A.; Fan, H. Y.; Qi, L.; Kushima, A.; Li, J. *Science* **2010**, *330*, 1515−1520.
(12) Zhang, L. Q.; Liu, X. H.; Liu, Y.; Huang, S.; Zhu, T.; Gui, L. J.; Mao, S. X.; Ye, Z. Z.; Wang, C. M.; Sullivan, J. P.; Huang, J. Y. *ACS Nano* **2011**, *5*, 4800−4809.
(13) Liu, X. H.; Liu, Y.; Kushima, A.; Zhang, S. L.; Zhu, T.; Li, J.; Huang, J. Y. *Adv. Energy Mater.* **2012**, *2*, 722−741.
(14) Liu, X. H.; Zheng, H.; Zhong, L.; Huang, S.; Karki, K.; Zhang, L. Q.; Liu, Y.; Kushima, A.; Liang, W. T.; Wang, J. W. *Nano Lett.* **2011**, *11*, 3312−3318.
(15) Wang, Z. Y.; Zhou, L.; Lou, X. W. *Adv. Mater.* **2012**, *24*, 1903−1911.
(16) Shi, W. H.; Zhu, J. X.; Rui, X. H.; Cao, X. H.; Chen, C.; Zhang, H.; Hoon Hng, H.; Yan, Q. Y. *ACS Appl. Mater. Interfaces* **2012**, *4*, 2999−3006.
(17) Wang, D. N.; Li, X. F.; Yang, J. L.; Wang, J. J.; Geng, D. S.; Li, R. Y.; Cai, M.; Sham, T.; Sun, X. L. *Phys. Chem. Chem. Phys.* **2013**, *15*, 3535−3542.
(18) Wang, X.; Cao, X. Q.; Bourgeois, L.; Guan, H.; Chen, S. M.; Zhong, Y. T.; Tang, D. M.; Li, H. Q.; Zhai, T. Y.; Li, L.; Bando, Y.; Golberg, D. *Adv. Funct. Mater.* **2012**, *22*, 2682−2690.
(19) Yin, J. F.; Cao, H. Q.; Zhou, Z. F.; Zhang, J. X.; Qu, M. Z. *J. Mater. Chem.* **2012**, *22*, 23963−23970.
(20) Xie, D.; Yuan, W. W.; Dong, Z. M.; Su, Q. M.; Zhang, J.; Du, G. H. *Electrochim. Acta* **2013**, *92*, 87−92.
(21) Gu, Y.; Xu, Y.; Wang, Y. *ACS Appl. Mater. Interfaces* **2013**, *5*, 801−806.
(22) Li, J.; Dahn, J. R. *J. Electrochem. Soc.* **2007**, *154*, A156−A161.
(23) Long, B. R.; Chan, M. K. Y.; Greeley, J. P.; Gewirth, A. A. *J. Phys. Chem. C.* **2011**, *115*, 18916−18921.
(24) Wang, C. M.; Xu, W.; Liu, J.; Zhang, J. G.; Saraf, L. V.; Arey, B. W.; Choi, D.; Yang, Z. G.; Xiao, J.; Thevuthasan, S.; Baer, D. R. *Nano Lett.* **2011**, *11*, 1874−1880.
(25) Ghassemi, H.; Au, M.; Chen, N.; Heiden, P. A.; Yassar, R. S. *ACS Nano* **2011**, *5*, 7805−7811.
(26) Su, Q. M.; Dong, Z. M.; Zhang, J.; Du, G. H.; Xu, B. S. *Nanotechnology* **2013**, *24*, 255705.
(27) Su, Q. M.; Chang, L.; Zhang, J.; Du, G. H.; Xu, B. S. *J. Phys. Chem. C* **2013**, *117*, 4292−4298.
(28) Su, Q. M.; Xie, D.; Zhang, J.; Du, G. H.; Xu, B. S. *ACS Nano* **2013**, *7*, 9115−9121.
(29) Liu, Y.; Zheng, H.; Liu, X. H.; Huang, S.; Zhu, T.; Wang, J. W.; Kushima, A.; Hudak, N. S.; Huang, X.; Zhang, S. L. *ACS Nano* **2011**, *5*, 7245−7253.
(30) Liu, X. H.; Wang, J. W.; Liu, Y.; Zheng, H.; Kushima, A.; Huang, S.; Zhu, T.; Mao, S. X.; Li, J.; Zhang, S. L. *Carbon* **2012**, *50*, 3833−3844.
(31) Su, Q. M.; Du, G. H.; Zhang, J.; Zhong, Y. J.; Xu, B. S.; Yang, Y. H.; Neupane, S.; Kadel, K.; Li, W. Z. *ACS Nano* **2013**, DOI: 10.1021/nn405254n.
(32) Xie, J.; Liu, S. Y.; Cao, G. S.; Zhu, T. J.; Zhao, X. B. *Nano Energy* **2013**, *2*, 49−56.

(33) Liu, X. H.; Zhong, L.; Huang, S.; Mao, S. X.; Zhu, T.; Huang, J. Y. *ACS Nano* **2012**, *6*, 1522−1531.
(34) Wang, X.; Tang, D. M.; Li, H. Q.; Yi, W.; Zhai, T. Y.; Bando, Y.; Golberg, D. *Chem. Commun.* **2012**, *48*, 4812−4814.
(35) Wang, F.; Yu, H. C.; Chen, M. H.; Wu, L. J.; Pereira, N.; Thornton, K.; Van der Ven, A.; Zhu, Y. M.; Amatucci, G. G.; Graetz, J. *Nat. Commun.* **2012**, *3*, 1201.